Analysis of Carbon Sequestration Pattern in Tropical Fruit Trees

G. Arulselvi
Assistant Professor
Department of CSE
FEAT, Annamalai University
Annamalainagar-608 002, India.

V. Ramalingam
Professor
Department of CSE
FEAT, Annamalai University
Annamalainagar-608 002, India.

S. Palanivel
Associate Professor
Department of CSE
FEAT, Annamalai University
Annamalainagar-608 002, India.

ABSTRACT

Terrestrial carbon sequestration is an important pathway of minimizing CO_2 concentration in the atmosphere. Tropical evergreen trees like cashew have some adaptive mechanism in an environment with strong seasonal variation of light and water.In this study, multilayer satellite images from the vegetation (VGT) sensors on board the Spot satellite (01/2006 to 12/2009) for Cashew plantations areas of Tamilnadu, India were analyzed for temporal variability. The temporal analysis of vegetation indices was done and the GPP (Gross Primary Productivity) was calculated using the satellite based vegetation photosynthesis model (VPM). The enhanced vegetation index (EVI) identified subtle changes in the seasonal dynamics of leaf phenology in Cashew plantation area, as supported by leaf moisture content and leaf area index. The land surface water index (LSWI), indicates that the plantation experienced water stress during the dry seasons. The VPM model which uses EVI, LSWI and site specific climate data for 2008-2009 predicted high GPP in the late wet season than in summer season. The GPP calculated from the remote sensing data are classified into three classes using Radial Basis Function Neural Network (RBFNN). The calculated GPP of different months in a year showed that the monthly GPP ranged from 50-128 g C/m2. The RBFNN is trained to provide an output value of 0, 1 and 2 for carbon sequestration which ranged from 50-75, 76-100 and 101-125 g C/m2, respectively. The experimental results shows that the RBFNN classifies the carbon sequestration with an accuracy of 95.2%.

Key words

Carbon sequestration, Pattern classification, Radial Basis Function Neural Network (RBFNN), Cashew, Gross Primary Production (GPP).

1. INTRODUCTION

Global warming is amongst the most dreaded problems of the new millennium. Green house gas is supposedly the strongest casual factor for global warming. One of the options for reducing the rise of green house gas concentration in the atmosphere and thus possible climate change is to increase the amount of carbon removed by and stored in plants. Forests are large reservoirs of carbon as well as potential carbon sink and sources to the atmosphere. In tropical countries like India, forest carbon sinks are believed to offset a significant portion of carbon emission associated with fossil fuel combustion. But due to large scale industrialization and increased population, the forest area is slowly declining. Perennial fruit trees like Cashew, Mango and Guava have similar potential like forest trees to sink atmospheric carbon. Cashew is an evergreen fruit tree; it occupies nearly 40,000 ha in Tamilnadu and has great potential for carbon sequestration. In India, Cashew is grown in seasonally moist tropical climate having a distinct dry and wet season. There is a strong seasonality of Photosynthetically Active Radiation (PAR) usually being much larger in late wet season than in the dry season. The seasonally moist tropical fruit trees have evolved two adaptive mechanisms to maximize carbon uptake in an environment with large seasonal variation of light and water. One adaptive mechanism is that perennial fruit trees have deep roots (1.0 m and deeper) for getting access to water in deep soil during dry season. In Cashew plantation, the dry season evaporation was 4.5 mm/day while the wet season evaporation was 3.1 mm/day.

In Cashew plantations the new leaf formation started during the onset of rainy season i.e. during the month of October which coincides with the start of winter season. In this study, the analysis of satellite images with meteorological data was combined. The objectives of this study are to estimate the seasonal dynamics of carbon sequestration in the tropical Cashew plantation area of Tamilnadu, India using Vegetation Photosynthetic Model (VPM) and to explore the capability of Radial Basis Function Neural Network (RBFNN) to classify the pattern of Carbon Sequestration in the Cashew plantation on the basis of quantity of carbon sequestered in different periods.

2. VPM MODEL

The VPM model [1] takes advantages of additional spectral bands (Eg. blue, and short wave infrared (SWIR)) that are available from advanced optical sensors. VEGETATION (VGT) sensor is the new generation optical sensor on board the SPOT-4 satellite and it offers the potential for improved characterization of vegetation at the global scale. The input data to the VPM model are the enhanced vegetation index (EVI) [2], the land surface water index (LSWI) [3], air temperature, and PAR (Photosynthetically Active Radiation).

Over the last few decades, the time-series data of the normalized difference vegetation index (NDVI), which is calculated as the normalized ratio between red and near-infrared (NIR) bands, have been widely used in satellite based modeling of GPP and NPP of terrestrial vegetation [4]-[5]. The advanced very high resolution radiometer (AVHRR) sensors that have red and near-infrared (NIR) bands have provided multi-decadal time series of NDVI has several limitations, including saturation in a multilayer closed canopy and sensitivity to both atmospheric aerosols and the soil background [1], [6]. To account for these limitations of NDVI, the enhanced vegetation index (EVI) was developed [2].

$$NDVI = \frac{\rho_{nir} - \rho_{red}}{\rho_{nir} + \rho_{red}} \quad (1)$$

$$EVI = 2.5 \times \frac{\rho_{nir} - \rho_{red}}{\rho_{nir} + \left(6 \times \rho_{red} - 7.5 \times \rho_{blue}\right) + 1} \quad (2)$$

EVI includes the blue band for atmospheric correction, which is one important feature for the study in the forest area where seasonal burning of pasture and forest takes place throughout the dry season, either for agricultural purpose (land clearing) or natural fire events. The smoke and aerosols from the biomass burning could affect NDVI substantially, irrespective of vegetation changes. The advanced optical sensors (VGT) have additional spectral bands (e.g., blue and shortwave infrared), making it possible to develop time-series data of improved vegetation indices. EVI has recently been used for the study of temperate forests [3], [7], [8] and is much less sensitive to aerosols than NDVI [1]. As the short infrared (SWIR) spectral band is sensitive to vegetation water content and soil moisture, a combination of NIR and SWIR bands have been used to derive water sensitive vegetation indices [3], [9]- [10] including the land surface water index (LSWI) [3], [7], [11].

$$LSWI = \frac{\rho_{nir} - \rho_{swir}}{\rho_{nir} + \rho_{swir}} \quad (3)$$

As leaf liquid water content increases or soil moisture increases, SWIR absorption increases and SWIR reflectance decreases, resulting in an increase of LSWI value. Recent work in evergreen tropical forests has shown that LSWI is sensitive to changes in leaf water content over time [3], [12].

3. STUDY AREA

This research was conducted in Cashew plantation area of Tamilnadu, India. This area lies between 11º15′N to 11º43′N latitude and 79º16′E to 79º44′E longitude, and covers total area of 40,000 ha. The annual rainfall ranges from 700 mm to 900 mm with an average of 800 mm. October to December is the peak of wet season with mean monthly rainfall of 300 mm.

The study area has two rainfall regimes that are wet and dry seasons. The wet season stretches from October to January and the dry season ranges from February to September. The average mean temperature is 32^{o}C. The mean minimum temperature is 21.2^{o}C and the mean maximum temperature is 38^{o}C. The mean annual solar net radiation is 16.9MJm-2day-1, whereas the relative air humidity ranges from 70 to 80 percent with an average of 75 percent. The soil in the study area is characterized by neutral, deep, strongly weathered, moderately well drained. Inceptisols and Alfisoil are the dominant soil types in the study area. The elevation of the study area ranges from 300 to 500 MSL.

Field measurement is conducted in order to collect data such as leaf area index and leaf moisture content. Photosynthetic photon flux density is measured using portable photosynthetic system Li-6400. Temporal variability analysis is conducted to assess the temporal dynamics of Carbon Sequestration in the plantation area.

4. 10-DAY COMPOSITE IMAGES FROM THE VEGETATION SENSOR

The VEGETATION (VGT) sensor on board the SPOT-4 satellite is one of a new generation of space-borne optical sensors that were designed for the observation of vegetation and land surfaces. The VGT instrument has four spectral bands: blue (430-470 nm), red (610-680 nm), near-infrared (NIR, 780-890 nm), and shortwave infrared (SWIR, 1580-1750 nm). The blue band is primarily used for atmospheric correction. The SWIR band is sensitive to soil moisture, vegetation cover, and leaf moisture content. Unlike scanner sensors (e.g., AVHRR, MODIS), the VGT instrument uses the linear-array technology (push-broom), and thus produces high-quality images at moderate resolution (1 km) with greatly reduced distortion. Since its launch in March 1998, the VGT instrument has acquired daily images at 1-km spatial resolution for the globe. The VEGETATION Programme produces three standard VGT products: VGT - P (physical product), VGT-S1 (daily synthesis product) and VGT-S10 (10-day synthesis product). The spectral bands in the VGT-S1 products are estimates of ground surface reflectance, as atmospheric correction of ozone, aerosols and water vapor have been applied to the VGT-P images using the Simplified Method for Atmospheric Correction (SMAC) algorithm [13].

VGT-S10 data are generated by selecting the VGT-S1 pixels that have the maximum Normalized Difference Vegetation Index (NDVI) values within a 10-day period. The maximum NDVI value composite (MVC) approach helps minimize the effects of cloud cover and variability in atmospheric optical depth. There are three 10-day composites for 1 month: day 1-10, day 11-20, and day 21 to the last day of the month. The VGT-S10 products are freely available to the public (http://free.vgt.vito.be). The VGT-S10 data over the period of January 1-10, 2006 to December 21-31, 2009 for the globe was acquired. The NDVI, EVI and LSWI were calculated using the surface reflectance of blue (ρ_{blue}), red (ρ_{red}), nir (ρ_{nir}), and swir (ρ_{swir}) bands from the standard VGT-S10 data. A detailed description of the preprocessing and calculation of vegetation indices from the VGT-S10 data are provided in Xia et al., 2003. Cloudy observations in a time series of vegetation indices were gap-filled using a simple gap-filling method and the cloud quality flag in the VGT-S10 surface reflectance files [1]. In this study, 3×3 pixels (approximately 3×3km^2) that covered the

Vridhachalam meteorological station were selected for feature extraction and to calculate the GPP. The calculated GPP is classified using Radial Basis Function Neural Network.

5. RADIAL BASIS FUNCTION NEURAL NETWORK

The Radial Basis Function Neural Network (RBFNN) [14] has feedforward architecture with an input layer, a hidden layer, and an output layer as shown in Figure 1. Radial basis functions are embedded into a two-layer feed forward neural network. Such a network is characterized by a set of inputs and a set of outputs. In between the inputs and outputs, there is a layer of processing units called hidden units. Each of them implements a radial basis function. The input layer of this network has n_i units for a n_i dimensional input vector. The input units are fully connected to the n_i hidden layer units, which are in turn fully connected to the n_c output layer units, where n_c is the number of output classes. The activation functions of the hidden layer are chosen to be Gaussians, and are characterized by their mean vectors (centers) μ_i, and covariance matrices c_i, i = 1, 2, · · · , n_h. For simplicity, it is assumed that the covariance matrices are of the form $c_i=\sigma_i^2 I$, where i = 1,2, . . . n_h. Then the activation function of the i^{th} hidden unit for an input vector x_j is given by

$$g_{i(x_j)} = exp\left(\frac{-\|x_j - \mu_i\|^2}{2\sigma_i^2}\right) \qquad (4)$$

The μ_i and σ_i^2 are calculated by using suitable clustering algorithm. Here the k-means clustering algorithm is employed to determine the centers. The algorithm is composed of the following steps:

1. Randomly initialize the samples to k means (clusters) μ_1, · · · , μ_k
2. Classify n samples according to nearest μ_k.
3. Recomputed μ_k.
4. Repeat the steps 2 and 3 until no change in μ_k.

The number of activation functions in the network and their spread influence the smoothness of the mapping. The assumption $\sigma_i^2 = \sigma 2$ is made and σ2 is given in (5) to ensure that the activation functions are not too peaked or too flat.

$$\sigma^2 = \frac{\eta d^2}{2} \qquad (5)$$

In the above equation *d* is the maximum distance between the chosen centers and η is the empirical factor which serves to control the smoothness of the mapping function. Therefore, Eq. (4) is rewritten as

$$g_{i(x_j)} = exp\left(\frac{-\|x_j - \mu_i\|^2}{\eta d^2}\right) \qquad (6)$$

The hidden layer units are fully connected to the n_c output layer units through weights W_{ik}. The output units are linear, and the response of the k^{th} output unit for an input x_j is given by

$$y_k(x_j) = \sum_{i=0}^{N_H} w_{ik}\, g_i(x_j), k = 1,2,\ldots n_C \qquad (7)$$

Where g_0 (x_j)=1. Given n_t feature vectors from n_c classes, training the RBFNN involves estimating μ_i, i = 1, 2, · · · , n_h, η, d^2 and w_{ik}, i = 0, 1, 2, · · · , n_h, k = 1, 2, · · · , n_c. The training procedure is given below:

Determination of μ_i and d^2 : Conventionally, the unsupervised k-means clustering algorithm [17] can be applied to find n_h clusters from n_t training vectors. However, the training vectors of a class may not fall into a single cluster. In order to obtain clusters only according to class, the k-means clustering may be used in a supervised manner. Training feature vectors belonging to the same class are clustered to n_h/n_c clusters using the k-means clustering algorithm. This is repeated for each class yielding n_h cluster for n_c classes. These cluster means are used as the centers μ_i of the Gaussian activation functions in the RBFNN. The parameter d was then computed by finding the maximum distance between n_h cluster means.

Determining the weights w_{ik} between the hidden and output layer: Given that the Gaussian function centers and widths are computed from n_t training vectors, (7) may be written in matrix form as

$$Y=GW \qquad (8)$$

where Y is a $n_t \times n_c$ matrix with elements $Y_{ij} = y_j(x_i)$, G is a $n_t \times (n_h + 1)$ matrix with elements $G_{ij} = y_j(x_i)$, and W is a $(n_h + 1)\times n_c$ matrix of unknown weights. W is obtained from the standard least squares solution as given by

$$W = (G^T G)^{-1} G^T Y \qquad (9)$$

To solve W from (9), G is completely specified by the clustering results, and the elements of Y are specified as

$$Y_{ij} = \begin{cases} 1, & \text{if } x_i \in \text{class } j \\ 0, & \text{otherwise} \end{cases} \qquad (10)$$

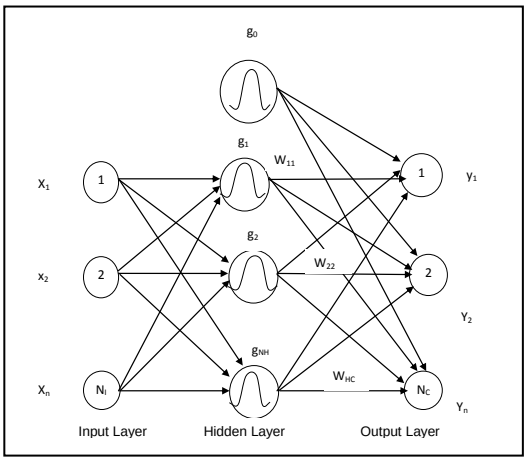

Fig 1: Radial Basis Function Neural Network

6. EXPERIMENTAL RESULTS

The seasonal dynamics of EVI as shown in Figure 2 is likely driven by a change in the leaf area index as the canopy of seasonally moist tropical Cashew plantation had varying LAI as shown in Figure 3 over seasons. We hypothesize that the seasonal distribution of EVI in a year may be attributed to both leaf fall of old leaves and emergence of new leaves resulting in dynamic changes in proportion of young and old leaves within a vegetation canopy over seasons. In general, the old leaves have less chlorophyll and water content but more structured material (Eg. lignin, cellulose) in comparison to young leaves which could lead to significant changes in absorbance, transmittance and reflectance of leaves as the aging process of leaves progress. The EVI continued to maintain higher value even up to February which may be attributed to continued emergence of new flushes in the winter season. The peak EVI values had the time lag of 2 months (January-February). The observed decrease of EVI in the peak dry season (May-June) could be largely attributed to aging process of leaves, including increase of both leaf thickness and the non-photosynthetic vegetation (NPV) component. This fact is supported by the field data. Field data collected at the experimental site showed that new leaf flush emergence starts during the end of September and continued up to January. The decrease in EVI from April to September may be attributed to both leaf age (older leaves) and epiphyll cover [20]. Young leaves have higher photosynthetic capacity than older leaves [15].

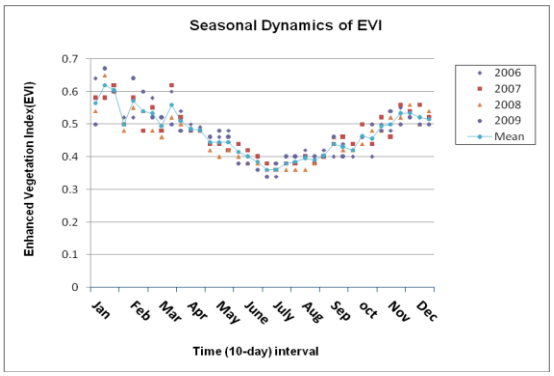

Fig 2: Seasonal Dynamics of Enhanced Vegetation Index (EVI)

Time series data (2006-2009) of LSWI was used to assess the status of leaf canopy water content of seasonally moist tropical Cashew plantation. LSWI values were generally higher in the wet season than in the dry season as shown in Figure 4. The seasonal dynamics of LSWI from 2006-2009 were positively correlated with that of leaf moisture content. The observed evapotranspiration data from the metrological research station were also higher in dry season than in the wet season as shown in Figure 4. The high LSWI values in the month of December-February might be due to high proportion of young leaves and more leaf water content as indicated by leaf moisture data and seasonal dynamics of EVI. Usually young leaves have more water content than old leaves [16]. The seasonal dynamics of LSWI shown that water stress exist in the experimental area during the dry season from 2006-2009.

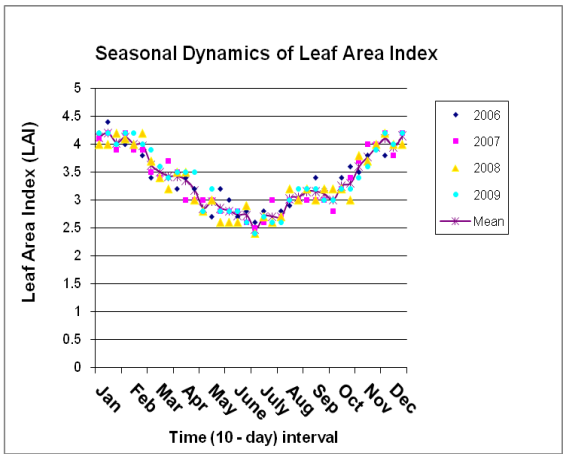

Fig 3: Seasonal Dynamics of LAI

6.1 Calculation of GPP in VPM model using 10 day VGT composites

VPM [3], [19] was used to estimate the GPP using LSWI, EVI and site specific climate (air temperature). As photosynthesis is closely coupled with water flux (we used observed water flux evapotranspiration) from the nearest metrological station in the experimental site to evaluate the performance of the VPM model as shown in Figure 6 The seasonal dynamics of predicted GPP agreed seasonably well with that of observed evapotranspiration. The VPM model predicts high GPP in the late wet season, as

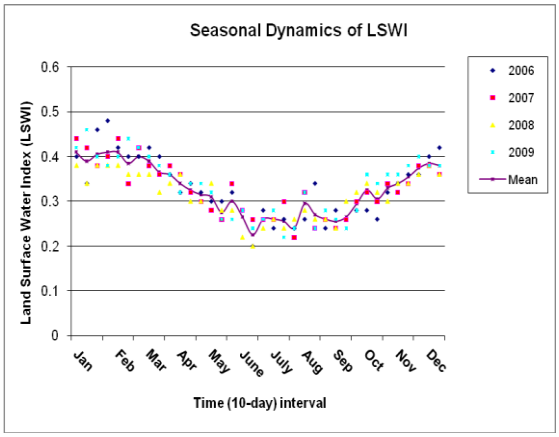

Fig 4: Seasonal Dynamics of LSW.

compared to dry season. For instance, the monthly GPP_{pred} was 104.29 g C/m^2 in January 2009 (wet season) but 62.71 g C/m^2 in June 2009 (dry season). Figure 5 shows that the relatively low GPP_{pred} in the dry season can be attributed to a number of factors. First the moisture stress in soil and maturity of leaves, secondly the averaged EVI value was lower (0.40) in late dry season (July-September) than in wet season (0.52) as shown in Figure 2. As EVI seasonal dynamics related to leaf phenology (leaf fall, leaf

emergence) at the canopy level. This suggests that leaf phenology could play an important role in the GPP calculation of seasonally moist tropical Cashew plantation. The annual sum of predicted GPP in Cashew plantation is (11967.811).

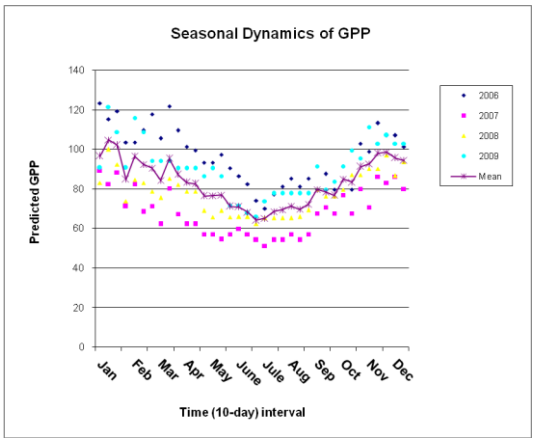

Fig 5: Seasonal Dynamics of Global Primary Productivity (GPP).

7. MODELING USING RBFN

Eleven features were extracted using both MODIS data and field observation at the rate of three per month in 10 locations from 2006-2009. So altogether 1440 samples were obtained. For RBFNN training, 850 samples out of 1440, each with 11 features are given as input to the RBFNN model. The RBF centers are located using k-means algorithm. The weights are determined using least squares algorithm. The value of k = 2, 4, 5 and 6 has been used in our studies. The system gives optimal performance for k = 6. For training, the weight matrix is calculated using the least squares algorithm discussed in Section 5. For classification the feature vectors are extracted and each of the feature vectors is given as input to the RBFNN model. The average output is calculated for each of the output neuron. The class to which the each sample belongs is decided based on the highest output. Figure 7 shows the performance of RBFNN for Carbon sequestration classification with number of training samples. Figure 8 shows the performance of RBFNN for different means. The performance of the system for RBFNN for Carbon sequestration classification is 95.2%.

8. CONCLUSION

In this study, seasonal dynamics of vegetation indices (EVI, LSWI and NDVI) from VGT sensor for a seasonally moist tropical Cashew plantation in Tamilnadu, India was evaluated for establishing the seasonal variation. Strong seasonal dynamics of EVI and LSWI from VGT was observed at the experimental site. In this study, our explanation for the seasonal dynamics of EVI, LSWI focus primarily on leaf phenology, leaf age, and leaf moisture content. As compared to other production efficiency model (PEM) that are based on NDVI-LAI-FAPAR relationship [18], the VPM model implements three hypothesis and alternate approaches in its model formulation [3]. The first hypothesis is the conceptual partitioning of PAV and NPV.

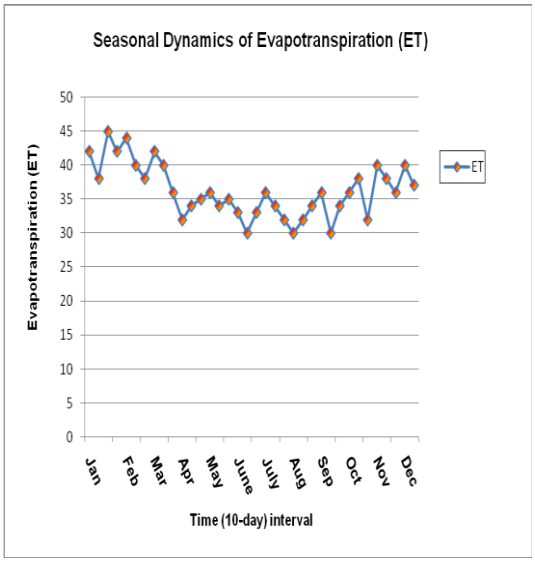

Fig 6: Seasonal Dynamics of Evapotranspiration (ET).

Assumed that the advanced vegetation indices (Eg. EVI) were capable of tracking subtle changes in PAV and NPV at leaf level. In addition to canopy level structured changes (LAI, plant area index) of forest are usually has little changes.

Fig 7: Performance Curve for RBFNN

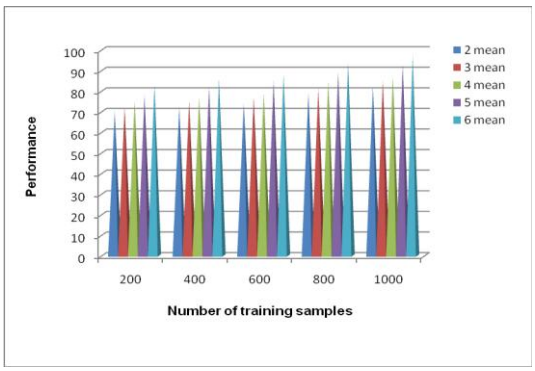

Fig 8: Performance of RBFNN for different means

7. REFERENCES

[1] X. Xiao, B. Braswell, Q. Zhang, S. Boles, S. Frolking, B. Moore, *Sensitivity of vegetation indices to atmospheric acrosols: Continental-scale observations in Northern Asia*, Remote Sensing of Environment. 84 (2003) 385–392.

[2] A. R. Huete, H. Q. Liu, K. Batchily, W. VanLeeuwen, *A comparison of vegetation indices global set of TM images for EOS-MODIS*, Remote Sensing of Environment. 59 (1997) 440 451.

[3] X. Xiao, D. Hollinger, J. D. Aber, M. Goltz, E. A. Davidson, Q. Y. Zhang, *satellite-based modeling of gross primary production in an evergreen needleleaf forest*, Remote Sensing of Environment. 89 (2004a) 519–534.

[4] C. B. Field, J. T. Randerson, C. M. Malmstrom, *Global net primary production-combining ecology and remote-sensing*, Remote Sensing of Environment. 51 (1995) 74–88.

[5] S. D. Prince, S. N. Goward, *Global primary production: A remote sensing approach*, Journal of Biogeography. 22 (1995) 815–835.

[6] A. Huete, K. Didan, T. Miura, E. P. Rodriguez, X. Gao, L. G. Ferreira, *Overview of the radiometric and biophysical performance of the MODIS vegetation indices*, Remote Sensing of Environment. 83 (2002) 195–213.

[7] S. Boles, X. Xiao, J. Liu, Q. Zhang, S. Munkhutya, S. Chen, *Land cover characterization of Temperate East Asia: Using multi-temporal image data of VEGETATION sensor*, Remote Sensing of Environment. 90 (2004) 477–489.

[8] X. Y. Zhang, M. A. Friedl, C. B. Schaaf, A. H. Strahler, J. C. F. Hodges, F. Gao, *Monitoring vegetation phenology using MODIS*, Remote Sensing of Environment. 84 (2003) 471–475.

[9] P. Ceccato, S. Flasse, S. Tarantola, S. Jacquemoud, J. M. Gregoire, *Detecting vegetation leaf water content using reflectance in the optical domain*, Remote Sensing of Environment. 77 (2001) 22–33.

[10] P. Ceccato, N. Gobron, S. Flasse, B. Pinty, S. Tarantola, *Designing a spectral index to estimate vegetation water content from remote sensing data: Part 1 Theoretical approach*, Remote Sensing of Environment. 82 (2002) 188–197.

[11] X. M. Xiao, S. Boles, J. Y. Liu, D. F. Zhuang, M. L. Liu, *Characterization of forest types in Northeastern China, using multi-temporal SPOT-4 VEGETATION sensor data*, Remote Sensing of Environment. 82 (2002) 335– 348.

[12] M. Maki, M. Ishiahra, M. Tamura, *Estimation of leaf water status to monitor the risk of forest fires by using remotely sensed data*, Remote Sensing of Environment. 90 (2004) 441–450.

[13] H. Rahman, G. Dedieu, SMAC: *A simplified method foratmospheric correction of satellite measurements in the solar spectrum*, International Journal of Remote Sensing. 15 (1994) 123–143.

[14] S. Haykin, Neural Networks: *A Comprehensive Foundation*, Pearson Education, Singapore, 2001.

[15] C. Field, *Leaf-age effects on stomatal conductance*. in E. Zeiger, G. Farquhar and I. R. Cowan (Eds), Global Biogeochemical Cycles. (1987) 367–384.

[16] D. A. Roberts, B. W. Nelson, J. B. Adams, F. Palmer, *Spectral changes with leaf aging in Amazon caatinga*, Trees-Structure and Function. 12 (1998) 315–325.

[17] Richard O. Duda, Peter E. Hart, and David G. Stork, *Pattern Classification*, JohnWiley-Interscience, New York, 2001.

[18] R. R. Nemani, C. D. Keeling, H. Hashimoto, W. M. Jolly, S. C. Piper, C. J. Tucker, *Climate-driven increases in global terrestrial net primary production from 1982 to 1999*, Science. 300 (2003) 1560–1563.

[19] X. Xiao, Q. Zhang, B. Braswell, S. Urbanski, S. C. Wofsy, *Modeling gross primary production of a deciduous broadleaf forest using satelite images and climate data*, Remote Sensing of Environment. 91 (2004) 256–270.

[20] A. Huete, P. Ratana, K. Didan, Y. Shimabukuro, H. Barbosa, L. G. Ferreira, *Seasonal biophysical dynamics along an Amazon eco-climatic gradient using MODIS vegetation indices*. anais Xi SBSR, Belo Horizonte, Brasil7 Instituto Nacional de Pesquisas Espaciais. 05-10 (2003) 665–672.